What is a comet?

Small bodies of the solar system

Lecture by Klaus Jockers, Göttingen, winter term 2004/2005

Comets1

What is a comet?

- The gas coma of comets
- Cometary spectra
- a General
- b Spectra in the UV and visual wavelength range
- c Spectra in the radio and microwave range (parent molecules)
- How to calculate production rates (appendix)


Comet Kohoutek in January 1972


Comet Halley in March 1986

Comet Hale-Bopp in March 1997

The Giotto probe approaches comet Halley on March 13, 1986

“Best” image of the nucleus of comet Halley as obtained with the Halley Multicolor Camera

Parts of a comet:

- Nucleus
- Coma
- Plasma tail
- Dust tail
- Hydrogen cloud

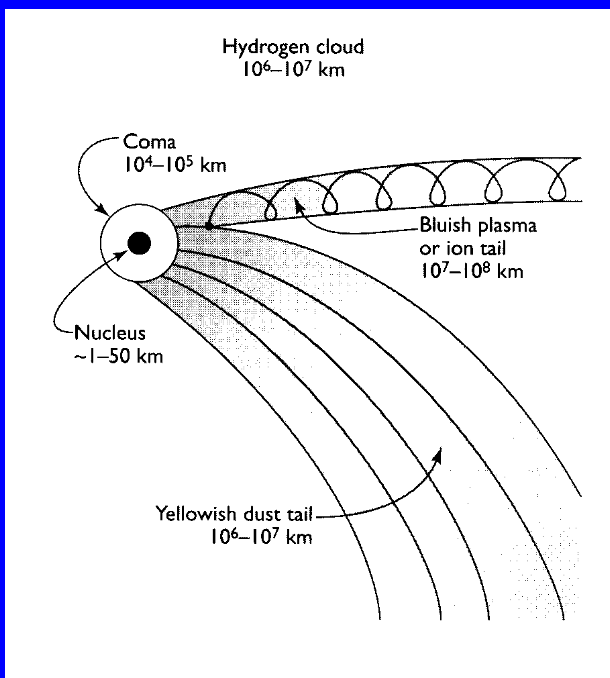

Parts of a comet, alternative picture.

As seen with the eye the plasma tail has blue color, because of the bands of CO^+ in the blue wave-length range.

The coma has the blue-green color of transitions of the C2 radical, similar to a Bunsen gas flame.

The dust tail has the color of the scattered solar light, i. e. very close to white.

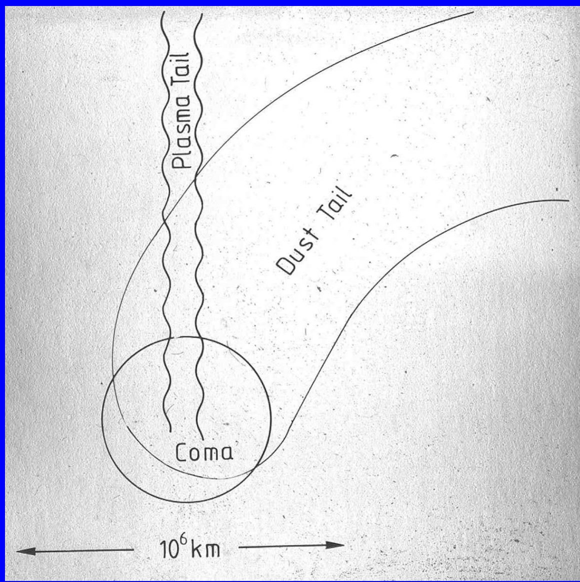

Comet P/Halley on March 16, 1986 imaged with Bochum wide-field camera

Red continuum + H_2O^+ | CO^+ at 426 nm | CN at 388 nm

Crovisier J., Solids and volatiles in comets: From cometary nuclei to cometary atmo-spheres, in Greenberg, Li eds., Formation and evolution of solids in space, Kluwer, 1999, 389-426.

TABLE 1. A selection of famous comets. Comets are listed by order of perihelion date for non-periodic or long-period comets, and by order of periodic comet number for short-period comets. For comets that appeared before 1995, the old-style provisional and definitive numberings are also given.

Comet			perihelion date	q [AU]
C/1882 R1 Great Comet	1882 II	1882b	17 Sep. 1882	0.00775
C/1965 S1 Ikeya-Seki	1965 VIII	1965f	21 Oct. 1965	0.00779
C/1969 Y1 Bennett	1970 II	1969i	20 Mar. 1970	0.538
C/1973 E1 Kohoutek	1973 XII	1973f	28 Dec. 1973	0.142
C/1975 V1 West	1976 VI	1975n	25 Feb. 1976	0.197
C/1980 E1 Bowell	1982 I	1980b	12 Mar. 1982	3.364
C/1983 H1 IRAS-Araki-Alcock	1983 VII	1983d	21 May 1983	0.991
C/1986 P1 Wilson	1987 VII	1986l	20 Apr. 1987	1.200
C/1989 X1 Austin	1990 V	1989c$_1$	10 Apr. 1990	0.350
C/1990 K1 Levy	1990 XX	1990c	24 Oct. 1990	0.939
C/1996 B2 Hyakutake			1 May 1996	0.230
C/1995 O1 Hale-Bopp			1 Apr. 1997	0.914
D/1993 F2 Shoemaker-Levy 9		1993e		
1P/Halley	1986 III	1982i	9 Feb. 1986	0.587
2P/Encke			23 May. 1997	0.331
21P/Giacobini-Zinner	1985 XIII	1984e	5 Sep. 1985	1.028
22P/Kopff			2 Jul. 1996	1.585
23P/Brorsen-Metcalf	1989 X	1989o	11 Sep. 1989	0.479
29P/Schwassmann-Wachmann 1				5.772
46P/Wirtanen			14 Mar. 1997	1.083
73P/Schwassmann-Wachmann 3			22 Sep. 1995	0.936
95P/Chiron			14 Feb. 1996	8.454
109P/Swift-Tuttle	1992 XXVIII	1992t	12 Dec. 1992	0.958

TABLE 3. Sublimation temperatures of selected cometary volatiles. Sublimation temperatures are given for a pure species in equilibrium with its own vapour, the total gas density being 10^{13} cm^{-3} with the listed relative abundance [X]/[H] of the given species. These temperatures are either taken from [110] (Y) or extrapolated from the Clausius-Clapeyon equation, using the data of the *Handbook of Chemistry and Physics* for species in the solid (S) or liquid (L) phase.

Species		log [X]/[H]	T_{subl}	Reference
anthracene	$C_{14}H_{10}$	−8	200	HCP(S)
phenanthrene	$C_{14}H_{10}$	−8	160	HCP(S)
naphtalene	$C_{10}H_8$	−8	160	HCP(S)
water	H_2O	−4	152	Y
hydrogen peroxide	H_2O_2	−7	128	HCP(S)
formic acid	HCOOH	−7	112	Y
acetic acid	CH_3COOH	−8	106	HCP(S)
ethanol	C_2H_5OH	−8	105	HCP(L)
benzene	C_6H_6	−8	104	HCP(S)
methanol	CH_3OH	−8	99	Y
hydrogen cyanide	HCN	−7	95	Y
methyl formate	CH_3OHCO	−8	95	HCP(L)
methyl cyanide	CH_3CN	−8	93	HCP

Sublimation temperature for different volatiles continued

sulphur dioxide	SO_2	−8	83	Y
ammonia	NH_3	−7	78	Y
carbon disulphide	CS_2	−8	78	HCP(L)
cyanoacetylene	HC_3N	−8	74	Y
carbon suboxide	C_3O_2	−8	73	HCP(L)
acetaldehyde	CH_3CHO	−8	73	HCP(L)
carbon dioxide	CO_2	−5	72	Y
propyne	CH_3CCH	−8	65	Y
formaldehyde	H_2CO	−8	64	Y
dimethyl ether	CH_3OCH_3	−8	60	HCP(L)
nitrous oxide	N_2O	−7	59	HCP(S)
hydrogen sulphide	H_2S	−7	57	Y
carbonyl sulphide	OCS	−8	57	HCP(L)
acetylene	C_2H_2	−8	54	HCP(S)
ethane	C_2H_6	−8	44	HCP
ethylene	C_2H_4	−8	38	HCP(L)
methane	CH_4	−4.5	31	Y
carbon monoxide	CO	−5	24	Y
dinitrogen	N_2	−4	22	Y
dihydrogen	H_2	0	5	Y

Energy balance of a cometary nucleus

$$\frac{1}{4}(1-A)\frac{F}{r^2} = (1-A_{\mathrm{IR}})\sigma T^4 + \frac{Q}{4\pi R^2}\frac{L}{N_0} + \text{heat conduction.}$$

$$\frac{Q}{4\pi R^2} = \frac{P(T)}{kT}\left(\frac{8kT}{\pi m}\right)^{1/2} = P(T)\left(\frac{8N_0}{\pi\mu kT}\right)^{1/2}$$

A : visual Albedo
A_{IR} : infrared Albedo
F : solar flux at 1 AU
r : distance sun - comet in AU
σ : Stefan - Boltzmann constant
T : temperature
Q : production rate in molecules s^{-1}

R : radius of nucleus
L : evaporation heat in Mol
N_0 : Avogadro's constant
$P(T)$: vapour pressure at phase transition
k : Boltzmann constant
m : mass of molecule
μ : molar weight of molecule

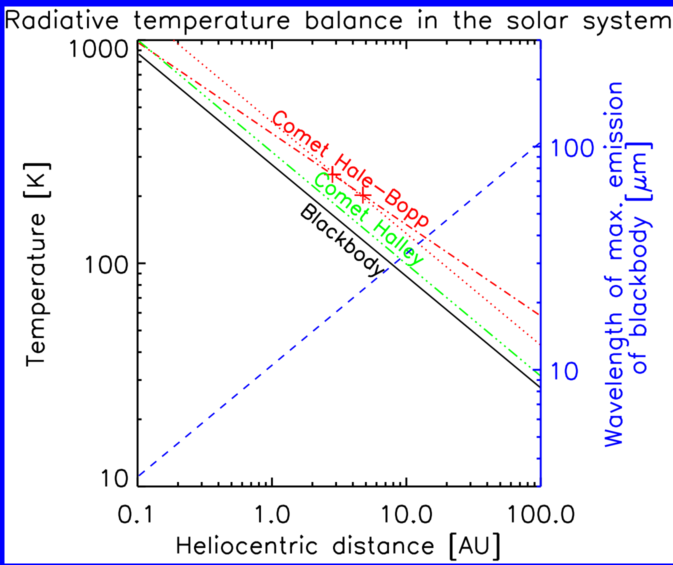

Z is the production rate per unit surface. At small heliocentric distances $Z \sim r_H^{-2}$, i.e. all absorbed solar energy goes into sublimation.

At large heliocentric distances the surface temperature < sublimation temperature and Z changes exponentially with r_H. The production rate depends on the thermal model of the nucleus and the location of the rotational axis.

As Z is the production rate per unit surface we can determine the nucleus size by comparing the observed production rates with the sublimation model.

Cowan JJ and A'Hearn MF, Moon and Planets 21, 155, 1979.

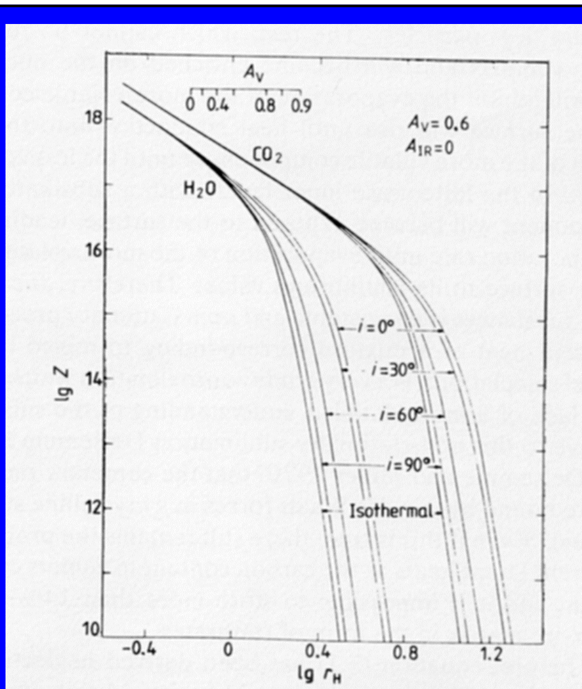

Irradiation of an asteroid by the Sun

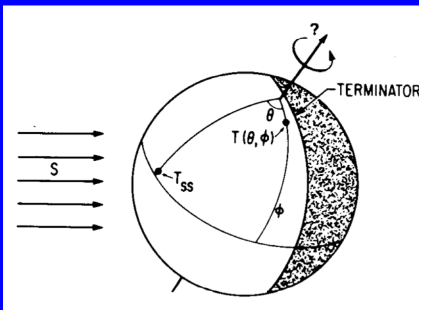

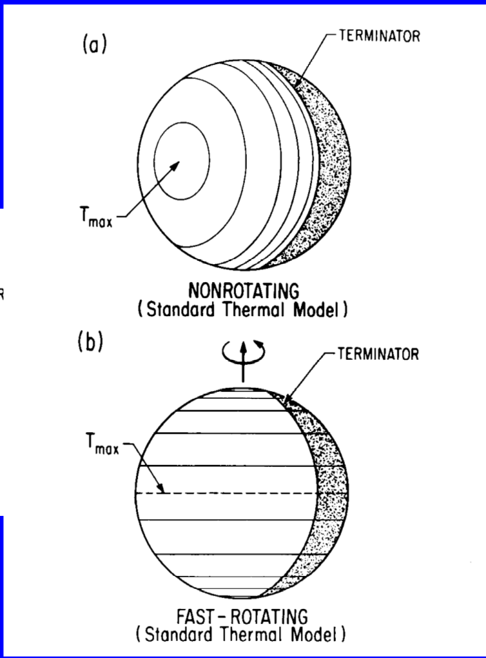

Lebofsky and Spencer, Asteroids II, Binzel et al. eds. U. of Arizona Press, Tucson, 1989, pp 128-147.

Biver et al.: The 1995-2002 long term monitoring of comet C/1995 O1 (Hale-Bopp) at radio wavelength. Earth, Moon and planets 90, 5-14, 2002.

Note cross-over of OH (dissociation product of water) and CO indicates that at large heliocentric distances, where water is frozen, CO can freely sublimate.

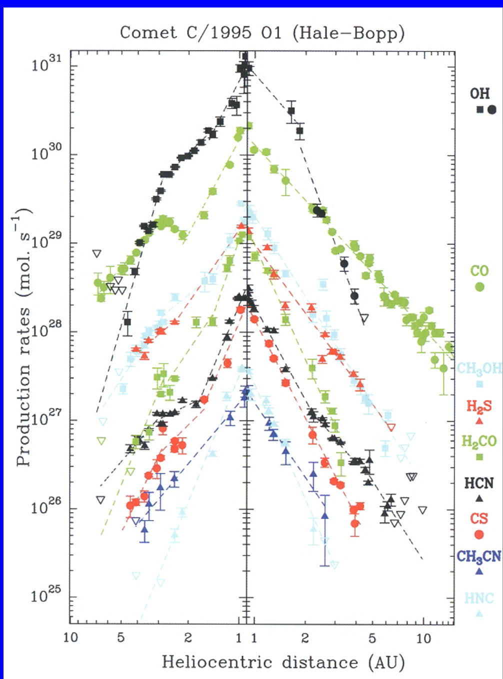

Crovisier J., in Greenberg, Li eds., Formation and evolution of solids in space, Kluwer, 1999, 389-426.

TABLE 4. Molecules observed in distant comets. Each entry gives the observation at the farthest distance r from the Sun at which the given molecule has been observed.

Comet	r [AU]	molecule	Q 10^{28} s^{-1}	reference
C/1980 E1 (Bowell)	5.2	OH	7.	[4]
	4.6	CN	0.00002	[4]
1P/Halley	4.8	CN	0.0003	[107]
	2.8	OH (radio)		[55]
	2.6	OH (UV)		[50]
95P/Chiron	11.3	$CN^{a)}$	0.14	[23]
		CO (radio)$^{a)}$		*IAUC* 6193
29P/Schwassmann-Wach. 1	5.8	CN	0.0008	[26]
	6.1	CO (radio)	4.	[34, 98]
	6.	CO^+		*several*
C/1995 O1 (Hale-Bopp)	6.7	CO (radio)	2.	[10, 69]
	6.8	CN	0.006	[54, 100]
	4.9	CH_3OH (radio)	0.09	*IAUC* 6382, [9]
	4.8	OH (UV)	1.5	[101]
	4.8	CS (UV)	0.012	[101]
	4.8	HCN (radio)	0.02	*IAUC* 6377
	4.7	OH (radio)	5.	[9]
	4.7	CO_2 (IR)	1.3	[36]
	4.6	C_2	0.05	[91]
	4.6	C_3		[91]
	4.3	H_2S (radio)	0.03	*IAUC* 6408, [9]
	4.3	NH_2		[91]
	4.1	CS (radio)	0.014	[9]
	4.1	H_2CO (radio)	0.01	[9]
	3.4	CH_3CN (radio)	0.012	[9]
	3.4	CO^+		*IAUC* 6468
	2.8	H_2O^+		[91]
	2.4	HNC		[9]

a) unconfirmed observation; see [92].

The gas coma of comets

Crovisier J., Solids and volatiles in comets: From cometary nuclei to cometary atmospheres, in Greenberg, Li eds., Formation and evolution of solids in space, Kluwer, 1999, 389-426.

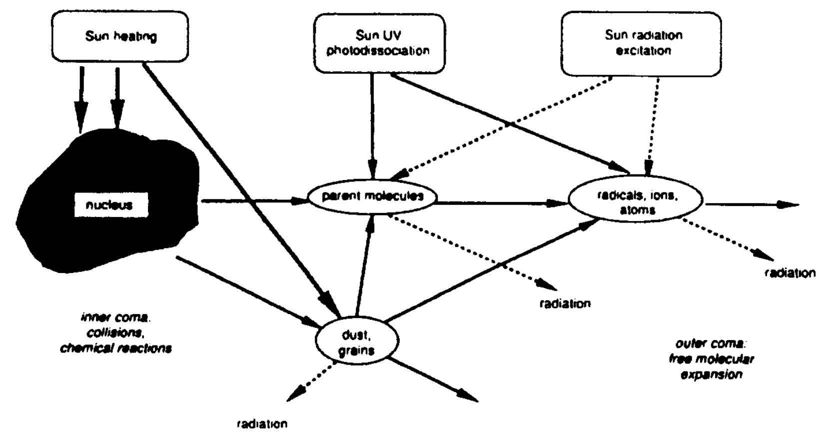

Figure 1. Physical and molecular processes initiated by solar radiation in comets.

Solar UV $\longrightarrow$ Photodissociation and Ionisation

Photodissociation: $AB + \text{photon} \rightarrow A + B + \text{energy}$

Not possible: $\cancel{AB + CD \rightarrow ABCD}$, $\cancel{A + B \rightarrow AB}$ } Energy set free by recombination can not be discharged

Possible: $AB + CD \rightarrow AC + BD$

Important reaction: $H_2O \rightarrow OH + H$ gets most of excess energy

$H_2O \rightarrow H_2 + O$

AB, CD molecules

Opacity of inner coma of a comet as function of wavelength in the UV spectral region. Giguere PT and Huebner WF 1978, Astrophys. J. 223, 638.

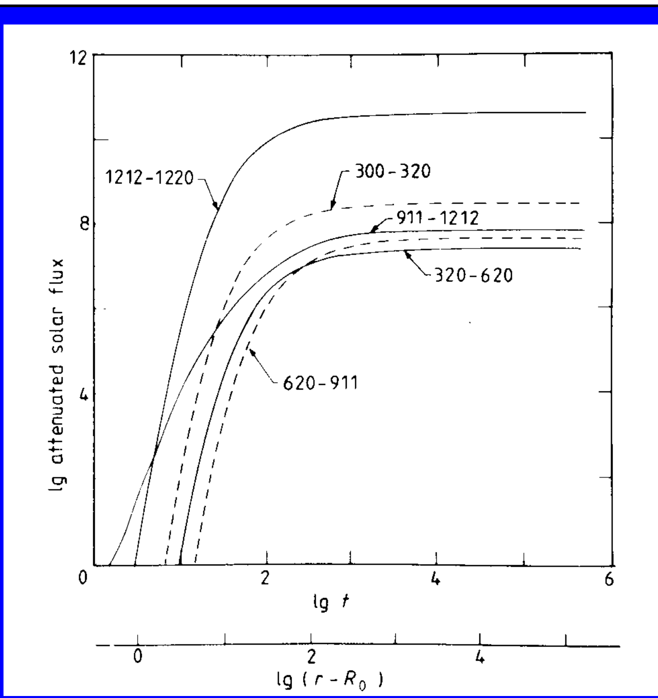

TABLE 5. Photo-destruction rates of cometary parent molecules for quiet Sun at 1 AU. Compiled from [32, 65], and references therein.

	Molecule		rate [s^{-1}]
water group:	water	H_2O	1.3×10^{-5}
	hydrogen peroxide	H_2O_2	1.3×10^{-4}
hydrocarbons:	methane	CH_4	8.0×10^{-6}
	acetylene	C_2H_2	1.4×10^{-5}
	ethylene	C_2H_4	4.8×10^{-5}
	ethane	C_2H_6	1.1×10^{-5}
	benzene	C_6H_6	1.1×10^{-3}
CO group:	carbon monoxide	CO	7.5×10^{-7}
	carbon dioxide	CO_2	2.0×10^{-6}
	carbon suboxide	C_3O_2	1.1×10^{-4}
CHO species:	formaldehyde	H_2CO	2.0×10^{-4}
	methanol	CH_3OH	1.3×10^{-5}
	formic acid	$HCOOH$	3.2×10^{-5}
	ethanol	C_2H_5OH	1.8×10^{-5}
	dimethyl ether	$(CH_3)_2O$	3.1×10^{-5}
	acetic acid	CH_3COOH	5.1×10^{-5}
nitrogen compounds:	ammonia	NH_3	1.5×10^{-4}
	hydrogen cyanide	HCN	1.5×10^{-5}
	cyanoacetylene	HC_3N	6.6×10^{-5}
	methyl cyanide	CH_3CN	6.7×10^{-6}
	isocyanic acid	$HNCO$	2.9×10^{-5}
sulphur compounds:	hydrogen sulphide	H_2S	2.5×10^{-4}
	carbon disulphide	CS_2	1.7×10^{-3}
	sulphur monoxide	SO	1.5×10^{-4}
	sulphur dioxide	SO_2	2.1×10^{-4}
	carbonyl sulphide	OCS	9.4×10^{-5}

Crovisier J., in Greenberg, Li eds., Formation and evolution of solids in space, Kluwer, 1999, 389-426.

Giguere PT and Huebner WF 1978, Astrophys. J. 223, 638.

Chemical model assuming radial outflow of neutrals and ions from the nucleus.

Note steep gradient of mother molecules H_2O and NH_3 as compared to daughter species and ions.

Chemical reactions are of type
$A + B \rightarrow C + D$
B may be a photon.

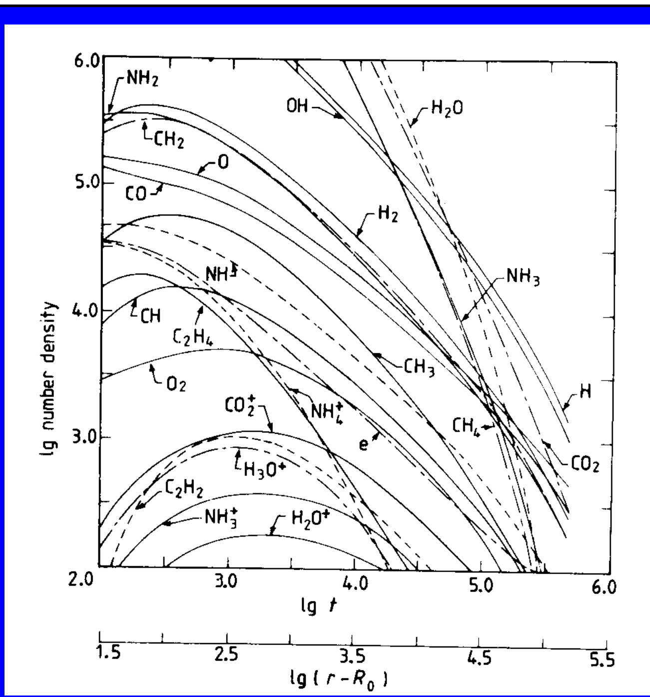

TABLE 6. Parent molecules in comets: the chronology of first detections.

Year	comet/technique	molecules
1973	C/1973 E1 (Kohoutek)	
	radio	HCN?
1976	C/1975 V1 (West)	
	UV	CO
1983	C/1983 H1 (IRAS-Araki-Alcock)	
	radio	NH_3?
	UV	S_2
1985–86	1P/Halley	
	radio	HCN, H_2CO?
	IR	H_2O, CO_2
1990	C/1989 X1 (Austin), C/1990 K1 (Levy)	
	radio	H_2CO, H_2S, CH_3OH
1996	C/1996 B2 (Hyakutake)	
	radio	NH_3, HDO, HNC, CH_3CN, OCS? HNCO?
	IR	CH_4, C_2H_2, C_2H_6
1997	C/1995 O1 (Hale-Bopp)	
	radio	OCS, HNCO, HC_3N, SO_2, HCOOH, H_2CS, NH_2CHO, $HCOOCH_3$

Crovisier J., in Greenberg, Li eds., Formation and evolution of solids in space, Kluwer, 1999, 389-426.

TABLE 9. Comparison of the abundances of ices in the interstellar medium (towards IRS9) and of cometary volatiles (at ~ 1 AU). Cometary abundances are from Table 7. ISM ice abundances are taken from a compilation of [97] from various sources as well as from recent *ISO* results [45, 105].

species	interstellar ices		cometary volatiles	
H_2O	=100		=100	
CO	10–40		2–20	
CH_3OH	5		1–7	
CO_2	10		2–6	
H_2CO	2–6	tentative	0.05–4	
HCOOH	3	tentative	~ 0.1	
CH_4	1–2		0.7	
other hydrocarbons	??		~ 1	C_2H_2, C_2H_6
NH_3	< 10		0.5	
O_3	$\lesssim 2$		??	
XCN	$\lesssim 0.5 - 2$		0.2	nitriles + HNCO
OCS, XCS	0.2		0.4	OCS + CS
SO_2	??		~ 0.1	
H_2	$>\sim 1$		??	
N_2	??		??	
O_2	??		??	

Crovisier J., in Greenberg, Li eds., Formation and evolution of solids in space, Kluwer, 1999, 389-426.

Cometary Spectra

Molecular spectra

Molecules have rotational lines in the far IR and microwave range, ro-vibrational transitions in the near IR and electronic transitions in the UV and visual wavelength range.

In the following these three types of spectra are briefly described, mostly from the point of view of energy quantization.

Angular momentum in many aspects is extremely important for molecular spectra, but can be mentioned here only to a minimal extent.

A strong molecular transition is a dipole transition, i. e. for a strong molecular transition the dipole moment of the molecule must change.

Section rules are a consequence of this.

Rotational levels:

$E_{rot} = [h^2 J(J+1)]/(8\pi^2 I)$

Note: individual rotational line are equidistant in frequency. The lower the momentum of inertia I the larger the distance between the lines.

Molecules with more than 2 atoms like water have more than one moment of inertia.

Symmetric or asymmetric top.
Water molecule is an asymmetric top.

Selection rules, allowed/forbidden transitions (electric dipole, magnetic dipole, quadrupole)
For rotation: $\Delta J = \pm 1$

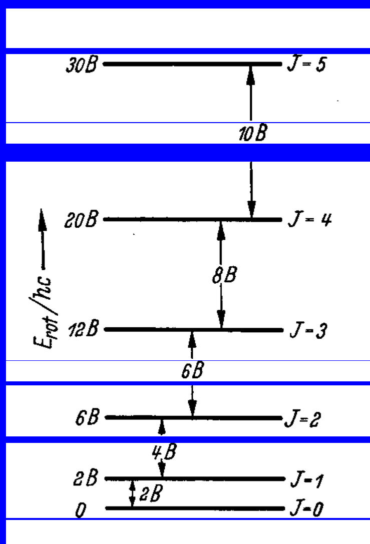

Abb. 203. Übergänge innerhalb des Rotationstermschemas des Elektronen- und Schwingungsgrundzustandes eines zweiatomigen Moleküls (Rotationsbande).

The wealth of water lines

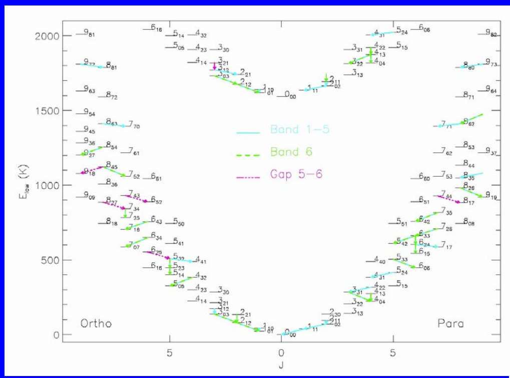

Energy Level Diagram

Submillimeter wavelength range

Water Spectrum

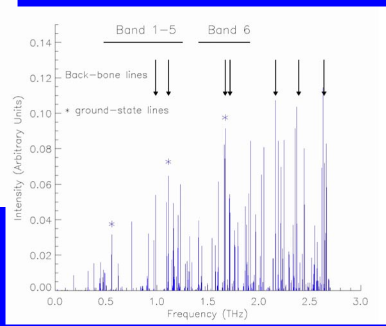

Oscillations:

Harmonic oscillator has equidistant energy levels.

Selection rule: $\Delta u = \pm 1$

The lines fall on top of each other.

Anharmonic oscillator:

Selection rule not strict, "hot" bands.

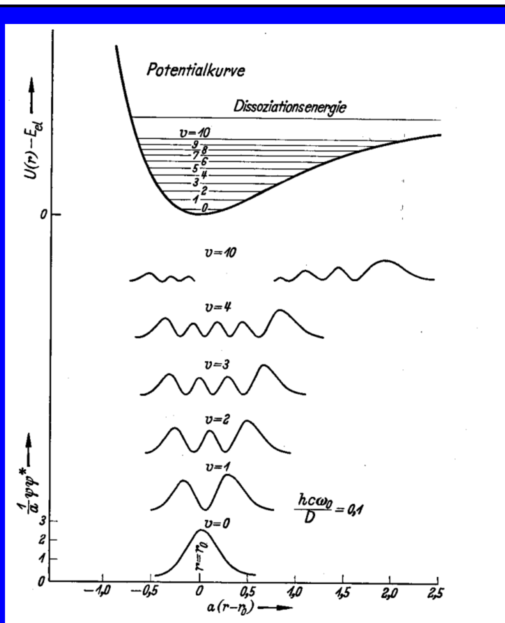

Abb. 189. Potentialkurve des anharmonischen Oszillators (Kraftansatz entsprechend dem bei zweiatomigen Molekülen in Näherung vorliegenden) und $\psi\psi^*$-Funktionen für eine Anzahl von Schwingungszuständen (nach GREGORY).

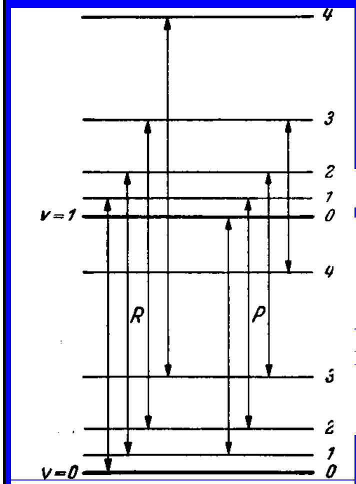

Abb. 204. Termschema mit Über-
tionsschwingungsbande eines zwei-

Allowed transitions: $\Delta J = \pm 1$

v_o (band origin) does not have a line: Zero gap.

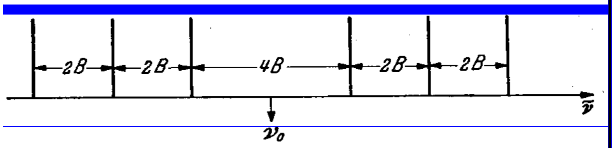

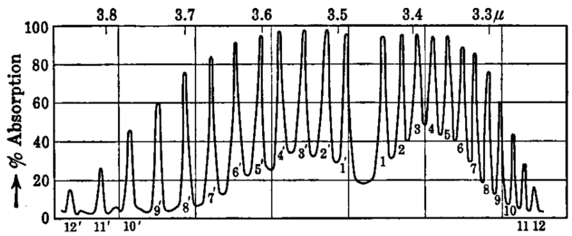

FIG. 32. **Fine Structure of the Principal Absorption Band (Fundamental) of HCl in the Near Infrared [after Imes (354)].** The ordinates give the percentage absorption, calculated from the galvanometer deflections. The numbers below the individual lines are the m values. The P branch is to the left, and the R branch is to the right. With still higher resolution [see Meyer and Levin (491) and Smith (1428)] each line is found to consist of two components on account of isotope effect (see Fig. 33 and p. 142).

$$\nu = \nu_0(\upsilon',\upsilon'') + B_{\upsilon'}\,J'(J'+1) - B_{\upsilon''}\,J''(J''+1)$$

$J' = J'' - 1$	P-Branch
$J' = J''$	Q-Branch
$J' = J'' + 1$	R-Branch

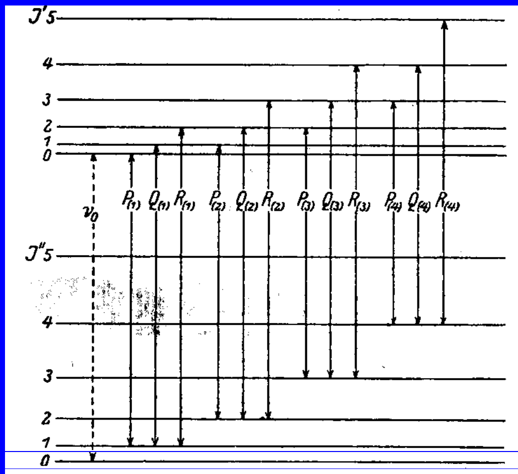

Abb. 206. Übergänge zwischen den Rotationstermfolgen zweier verschiedener Elektronenzustände eines zweiatomi-

Band heads:
Their "shading", i. e. the direction of bending of the Fortrat parabola, depends on the relation between $B_{\upsilon'}$ and $B_{\upsilon''}$

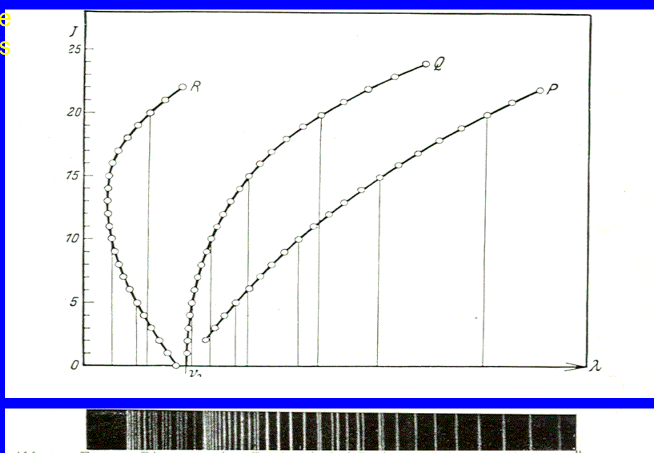

Abb. 207. FORTRAT-Diagramm einer Bande mit drei Zweigen und darunter die durch Überlagerung der Linien der drei Zweige entstehende ganze Bande im Spektrum (nach FERMI).

Franck-Condon Principle: Strength of vibrational transitions in electronic spectra

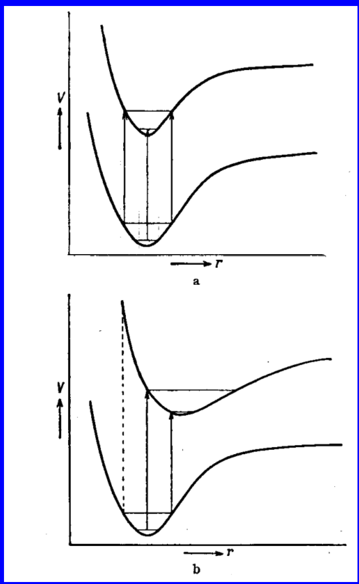

Case of similar binding force in both electronic states.
Example C_2

Case of reduced binding force in upper electronic state.
Example CO^+

Case of similar binding force in both electronic states.

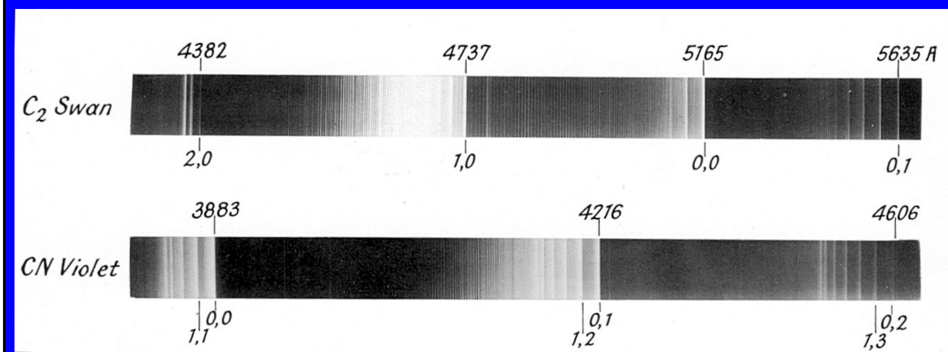

Case of reduced binding force in upper electronic state.

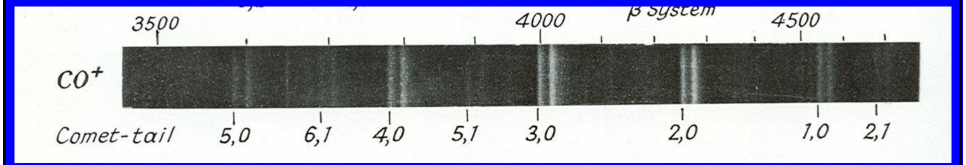

The doublets are spin doublets: A $^2\Pi_i \rightarrow X\ ^2\Sigma^+$

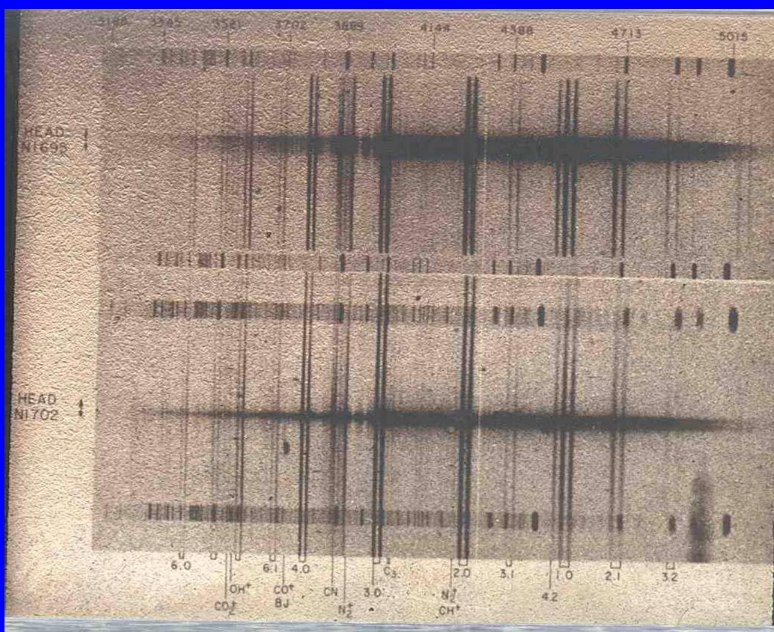

Fluorescence

Cometary molecules are most of all excited by fluorescence from the Sun. As the radiation is diluted, only low lying rotational or vibrational levels are occupied and provide a starting point for fluorescence.

The incoming photon must have a wavelength equal to the difference of two energy terms of the absorbing molecule. Relative speed between light source and molecule changes the frequency of the incoming photon as seen by the molecule and in this way may allow or inhibit absorption (Swings and Greenstein effects).

In comets the exciting radiation comes from the Sun.

The Sun has its maximum of output at 0.5 μm → $h\nu \approx 2.5$ eV.
Ly α = 121.5 nm → 10.2 eV. Lyman Continuum 91.1753 nm → 13.6 eV

Sun mostly excites electronic transitions. Excited molecule jumps immediately back to low lying level. Because $\Delta J = \pm 1$ are stronger transitions than $\Delta J = 0$, fluorescence pumps rotational levels. Rotational levels are “cooled” by purely rotational transitions in the mm wavelength range in much the same way as asteroid surfaces are cooled by thermal infrared radiation. Pure rotational transitions are forbidden in homonuclear molecules like C2, so fluorescence pumps rotation in this and other homonuclear molecules.

Swings Effect:
The relative motion between Sun and comet causes a Doppler shift of the solar spectrum at the comet. As the solar spectrum has a lot of absorption lines in the visual range (or some strong emission lines in the far UV), excitation of molecular radiation of the comet depends on its heliocentric velocity.

Swings effect (dependence of cometary emission on the heliocentric velocity v_H) illustrated using the example of OH emission at 309 nm:
Top: featureless solar spectrum.
Middle: v_H = -34.6 km s-1.
Bottom: v_H = 22.2 km s-1.

Fernandez & Jockers, Nature and origin of comets, Rep. Prog. Phys. 46, 665-772, 1983.

The Swings effect is also strong in the CN violet band because this band is present in the solar spectrum as well.

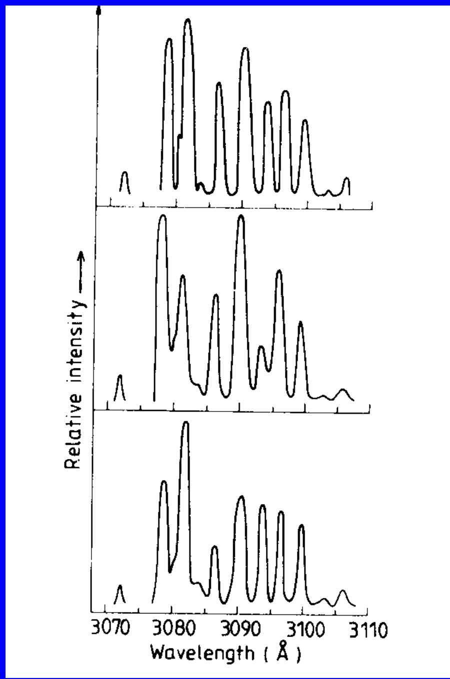

MF A'Hearn, in LL Wilkening ed. “Comets”, U. of Arizona Press, Tucson, 1983.

Dependence of fluorescence efficiency of CN and OH on heliocentric velocity of a comet.

As the CN band is present in absorption in the solar spectrum, we have the deep minimum at zero heliocentic velocity.

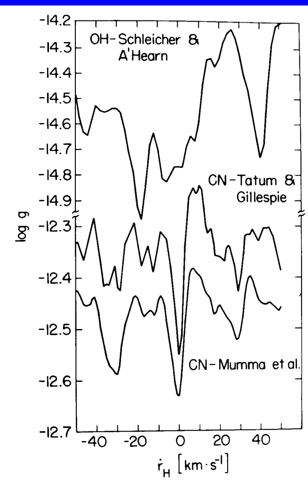

Fig. 4. Variation with heliocentric radial velocity of the logarithm of the fluorescence efficiency for OH (0–0 band) and CN (B–X; $\Delta v = 0$). Note the different ordinate scales for the two species. Because OH exhibits many fewer lines than does CN, the Swings effect is more pronounced. Differences between the two curves for CN are due to different molecular parameters (producing the overall shift) and the difference between the whole-disk solar spectrum used by Mumma et al. (1978) and the disk-center solar spectrum used by Tatum and Gillespie (1977). The shape of the radial velocity variation changes with heliocentric distance by amounts comparable to the difference in shape of the two curves exhibited here (results for OH from Schleicher and A'Hearn 1981).

Complicated organic molecules do not have electronic transitions and are destroyed (photodissociated) by solar radiation. They are excited by collisions or far IR radiation from the comet nucleus or other molecules.

Water does not have good stable electronic transitions. In comets vibration transitions are excited by solar infrared radiation.

Spectra in the UV and visual wavelength range
Solar spectrum
Cometary spectra

The solar spectrum in the Ultraviolet

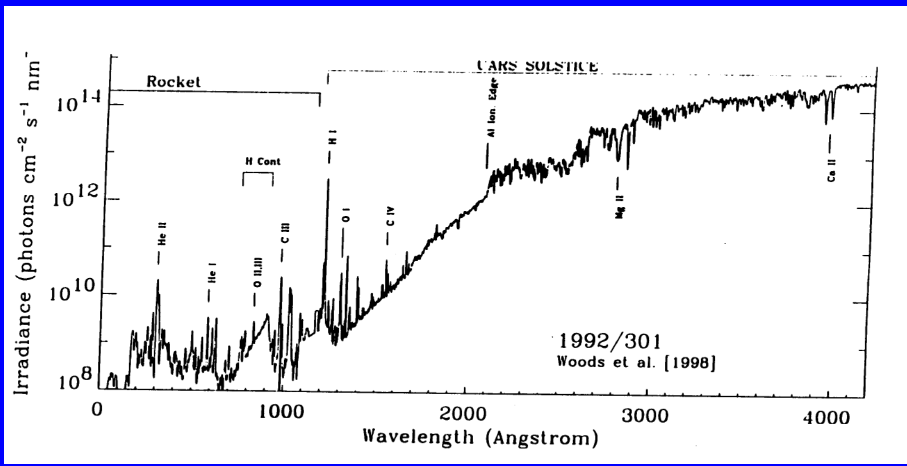

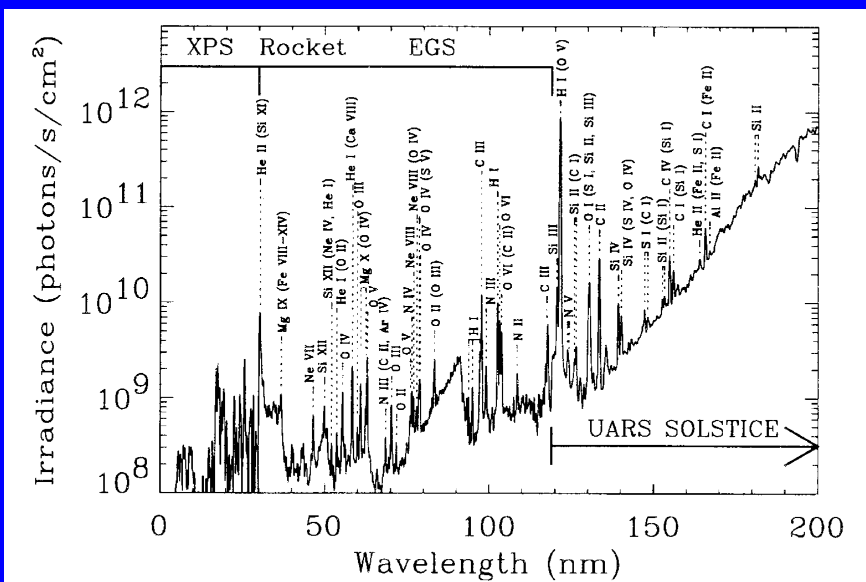

Solar VUV irradiance spectrum for Nov. 3, 1994. Labels in brackets are weaker blends.
Woods TN et al: Solar Phys. 177, 133-146, 1998.

The solar spectrum from 300-900 nm (Kitt Peak solar flux atlas)

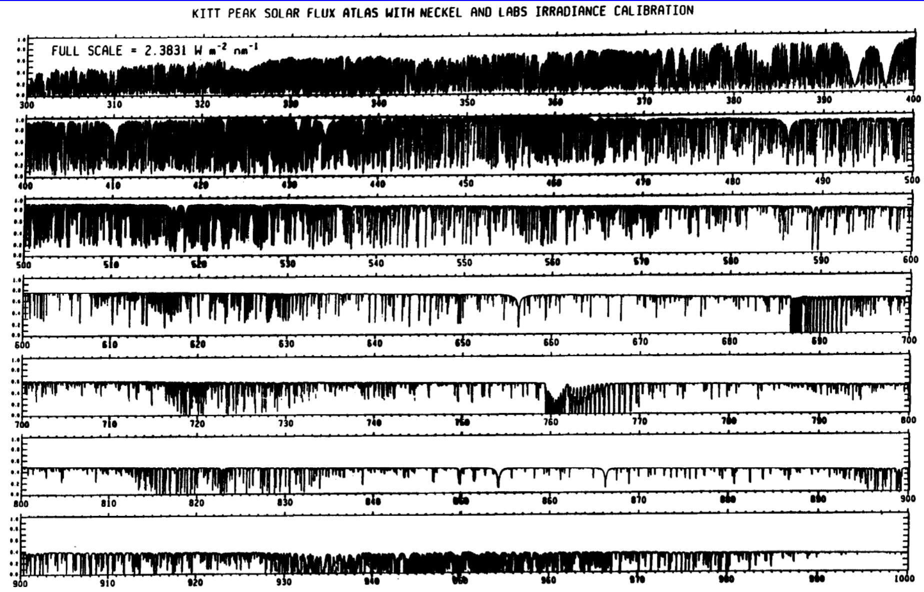

Figure 3. The absolute irradiance spectrum, the solar flux at the top of the atmosphere, derived from the Kitt Peak Solar Flux Atlas by normalizing it to the low-resolution irradiance measurements of Neckel and Labs. The wavelength range is 300 to 1000 nm. All the telluric oxygen and water lines must be edited out to determine the true irradiance.

Isodensity contours of the hydrogen cloud of comet West 1976 IV observed in Lyα by Opal and Carruthers (1977, Icarus 31 503). The contours are superposed on a visible picture of the comet taken by S. Koutchmy on the same day.

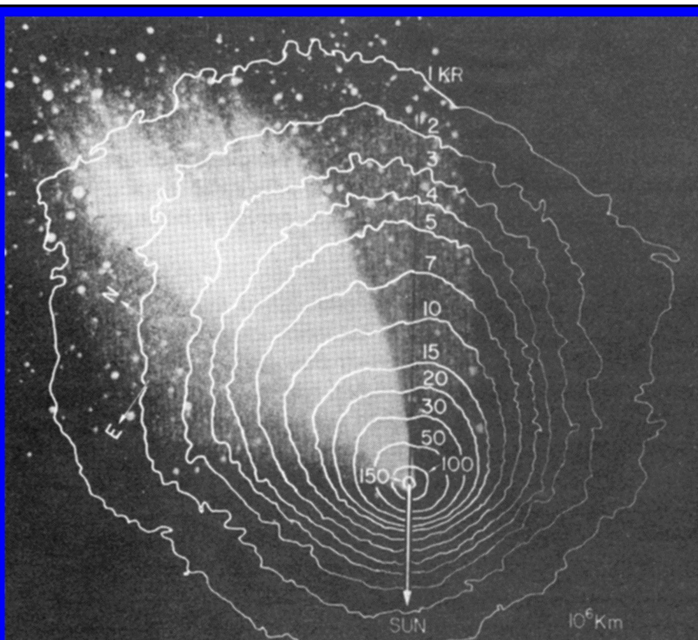

Fernandez & Jockers, Nature and origin of comets, Rep. Prog. Phys. 46, 665-772, 1983.

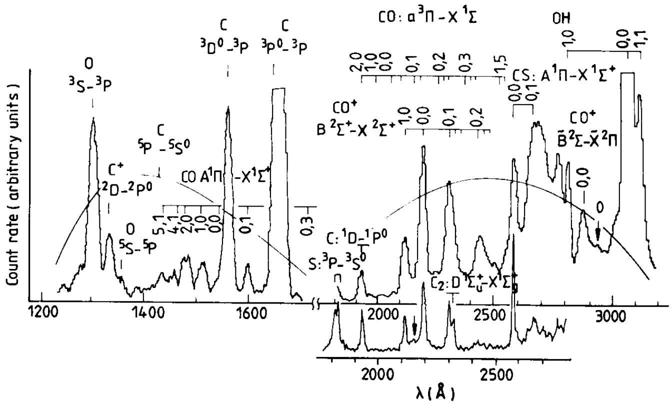

Figure 31. Ultraviolet spectra of comet West 1976 VI recorded with sounding rockets by Feldman and Brune (1976) on 5 March and Smith *et al* (1980) on 10 March 1976 (separate curve on bottom). The thin lines in the upper spectrum indicate the relative sensitivity of the detectors. The arrow at 2154 Å (bottom) points to the feature identified with the (0,1) transition of the Cameron band. The arrow at 2965 Å (top spectrum) indicates the forbidden O I transauroral lines.

Fernandez & Jockers, Nature and origin of comets, Rep. Prog. Phys. 46, 665-772, 1983.

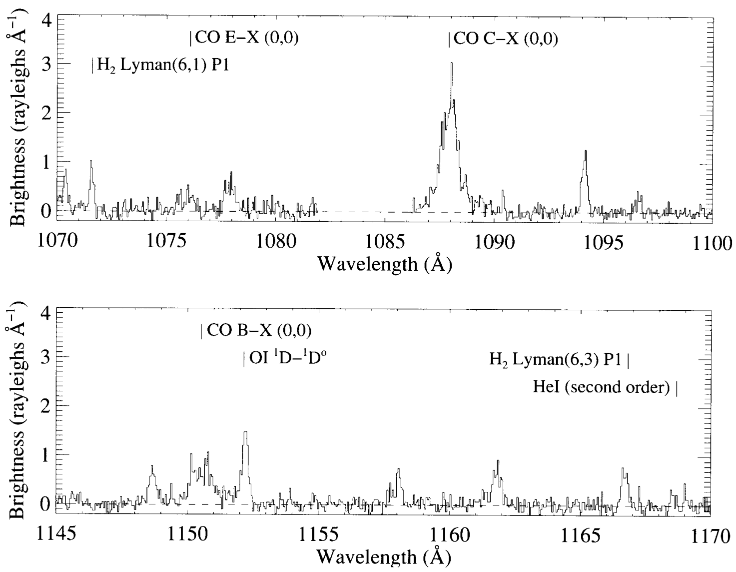

FIG. 1.—*FUSE* spectrum of comet C/2001 A2 (LINEAR) obtained beginning 2001 July 12.58 UT. Only data from orbital night (9535 s) are included to avoid terrestrial dayglow contamination. Data from the LiF1a and LiF2a channels are shown, rebinned to 0.054 Å intervals. The identified features are labeled.

Feldman PD, Weaver HA, Burgh EB, ASTROPHYS J 576: L91-L94, 2002

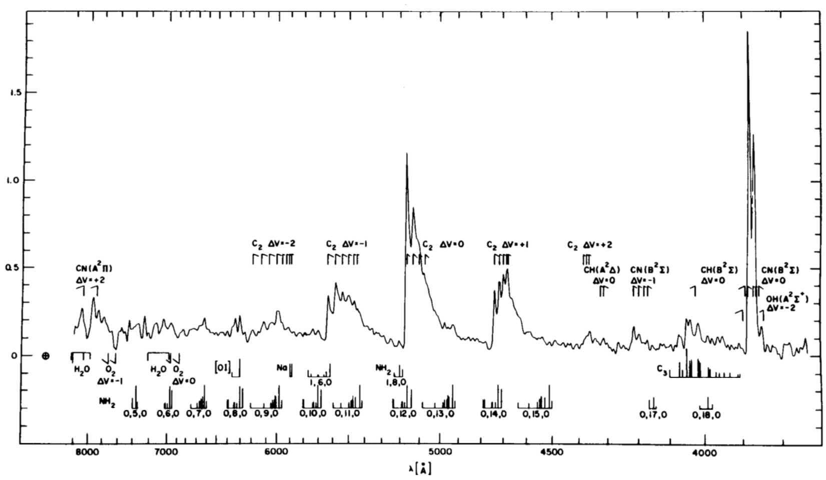

Fig. 1. Average of several spectra of Comet Kohoutek 1973 XII at 1 AU postperihelion. Radius of the circular aperture was 6.0 × 10^4 km. Band heads of the usually observed diatomic species are shown, as are the strongest lines (from theory and/or higher-resolution studies) of commonly observed triatomics and atoms even though not all are present in this spectrum. Telluric absorption features of O_2 and H_2O are also shown (from A'Hearn 1976).

Spectrum of Comet Kohoutek 1973 XII at 1 AU postperihelion in the visual and near-infrared wavelength range. Note molecular band structure. The C2 molecule dominates the visual spectrum and gives the coma the color of the Bunsen flame. MF A'Hearn, in LL Wilkening ed. "Comets", U. of Arizona Press, Tucson, 1983.

MF A'Hearn, in LL Wilkening ed. "Comets", U. of Arizona Press, Tucson, 1983.

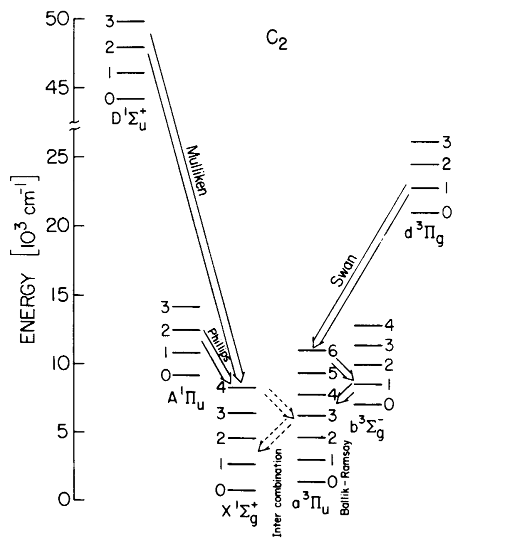

Fig. 3. Energy level diagram for C_2 showing several vibrational levels (numbered by vibrational quantum number) for each electronic state thought important in comets; numerous other states are omitted. The Ballik-Ramsay bands, not yet observed in comets, are important in controlling the vibrational populations because the higher vibrational states of a $^3\Pi_u$ can decay to lower vibrational states of $b^3\Sigma_g^-$. The intercombination transitions have not been observed either in comets or in the laboratory.

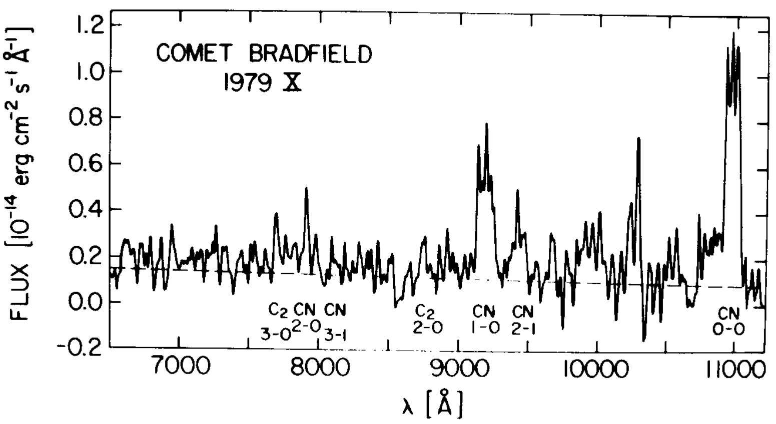

Fig. 2. Near-infrared spectral scan of nuclear region of Comet Bradfield 1979 X at 1 AU postperihelion. Aperture was ~ 1.4 by 2.7 X 10^3 km. Telluric and solar features have been removed by ratioing with a similar scan of a standard region on the Moon. The bands of the red system of CN and two Phillips bands of C_2 are shown. (Spectrum was provided by E.S. Barker.)

MF A'Hearn, in LL Wilkening ed. "Comets", U. of Arizona Press, Tucson, 1983.

Comet C/1961 R1 Humason (1962 VIII) observed by EH Geyer (University of Bonn) in Boyden Observatory, South Africa. The comet was at a heliocentric distance > 2 AU.

This is one of the exceptional CO rich comets.

The next slide shows its spectrum. Note strong double bands of CO^+, comparatively weak CN band, and absence of C_2 emission at 4700 Å. (Greenstein JL, Astrophys. J. 136, 688)

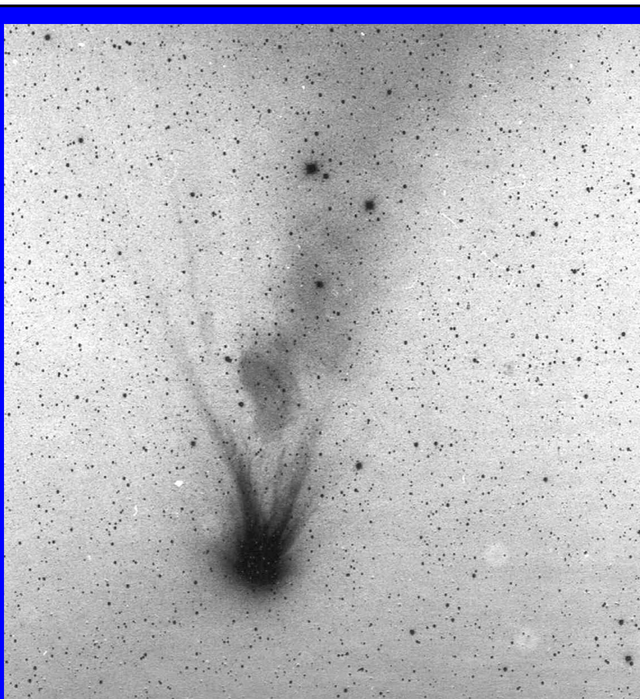

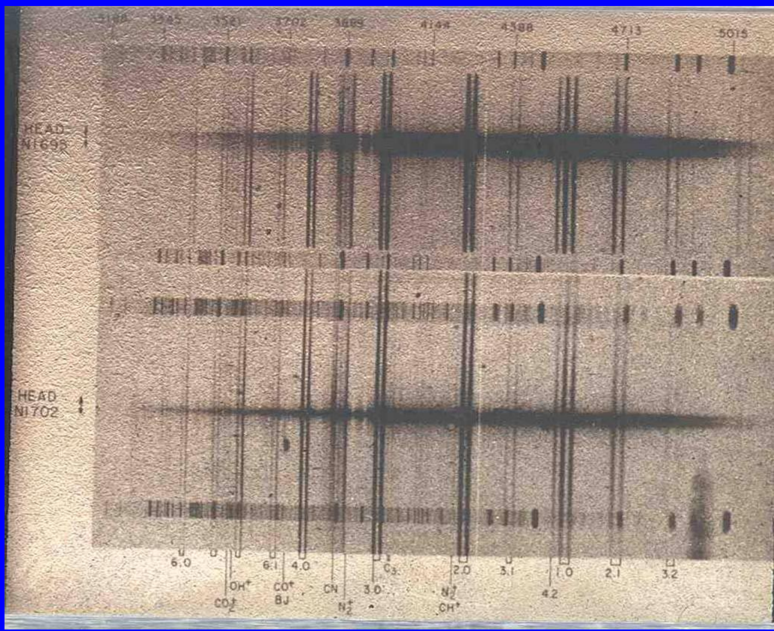

K. Jockers, A. Haenel, Observations of comet Halley with the focal reducer and multi-slit spectrograph of Hoher List Observatory at the ESO 1m telescope (unpublished).

Note the appearance of the emission of the tail ion CO^+ tailward and sunward of nucleus.

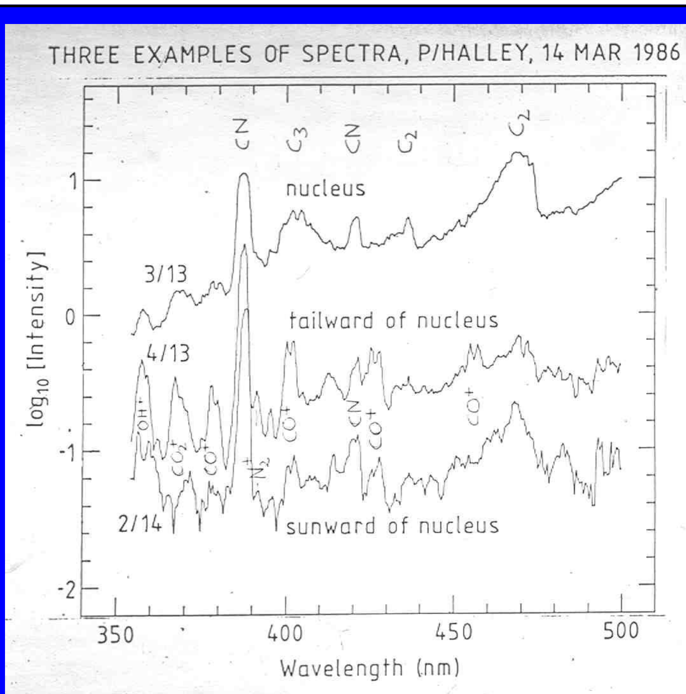

Spectra in the radio and microwave range (Parent molecules)

Crovisier J., Solids and volatiles in comets: From cometary nuclei to cometary atmo-spheres, in Greenberg, Li eds., Formation and evolution of solids in space, Kluwer, 1999, 389-426.

TABLE 7. Abundances of cometary volatiles. This table has been established from [12,31] and from the preliminary reports given in the *IAU Circ.* for the results on comets C/1996 B2 (Hyakutake) and C/1995 O1 (Hale-Bopp).

molecule	abundance (a)	method (b)	Nb (c)	comments
H_2O	=100.	IR	6	also indirect (from OH, O, H)
HDO	0.05	radio	2	
CO	2–20.	UV, radio, IR	> 5	extended source?
CO_2	2–6.	IR	2	
H_2CO	0.05–4.	radio	> 5	extended source
CH_3OH	1–7.	radio, IR	> 5	
HCOOH	~ 0.1	radio	1	
HNCO	0.07	radio	2	
NH_2CHO	~ 0.1	radio	1	
$HCOOCH_3$	0.05	radio	1	
CH_4	0.7	IR	2	
C_2H_2	0.3–0.9	IR	2	
C_2H_6	0.4	IR	2	
NH_3	0.5	radio	3	also indirect (from NH, NH_2)
HCN	0.1–0.2	radio, IR	> 5	
HNC	0.01	radio	2	
CH_3CN	0.01	radio	2	
HC_3N	0.01	radio	1	
H_2S	0.3	radio	> 5	
H_2CS	0.01	radio	1	
CS	0.1	UV, radio	> 5	from CS_2?
OCS	0.3	radio	2	
SO	~ 0.5	radio	1	from SO_2?
SO_2	~ 0.1	radio	1	
S_2	0.005–0.2	UV	2	

(a) abundance relative to water (100); listed abundances may be uncertain by a factor of 2 or more for some species.
(b) method of observation.
(c) number of comets in which this species was reliably and directly observed.

Crovisier J ., Solids and volatiles in comets: From cometary nuclei to cometary atmospheres, in Greenberg, Li eds., Formation and evolution of solids in space, Kluwer, 1999, 389-426.

Simultaneous observations of several rotational transitions allow the determination of temperature.

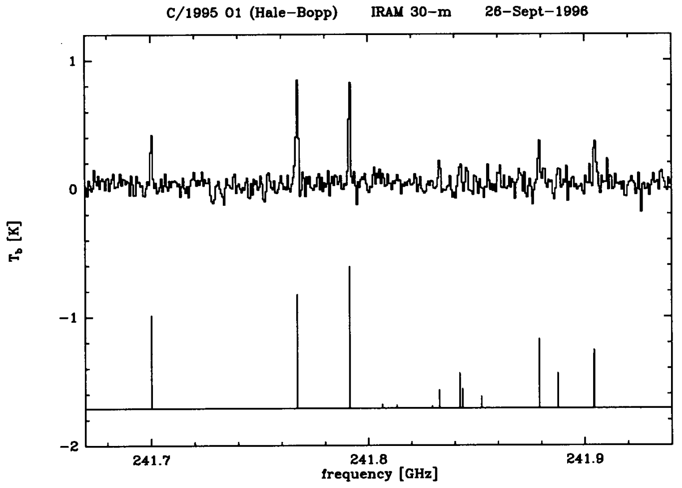

Figure 4. The lines of methanol around 242 GHz observed at IRAM in comet C/1995 O1 (Hale-Bopp), from which an accurate rotational temperature can be determined (from [11].)

HCN (full line, scaled down by a factor of 10) and its isomer HNC (dotted line) observed in Comet C/1996 B2 (Hyakutake) with two different radio telescopes). In equilibrium HNC should be totally absent. The observed ratio HNC/HCN = 0.06 equals the value observed in the interstellar medium. One way to produce HCN and HNC in equal amounts is dissociative recombination of $HCNH^+$ (protonated HCN).

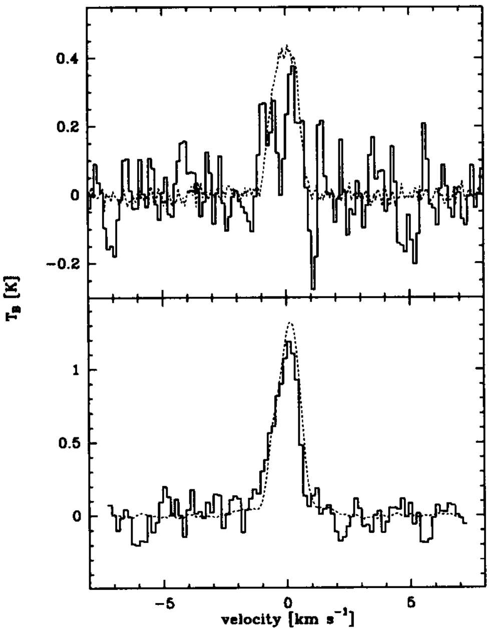

The line profiles presented here show strong sunward jets in Comet P/Swift-Tuttle at 1AU and Comet P/Schwassmann-Wachmann 1 at 6 AU from the Sun. Note reduced line width of P/SW1 because of reduced coma temperature at 6AU.

Crovisier J., Solids and volatiles in comets: From cometary nuclei to cometary atmo-spheres, in Greenberg, Li eds., Formation and evolution of solids in space, Kluwer, 1999, 389-426.

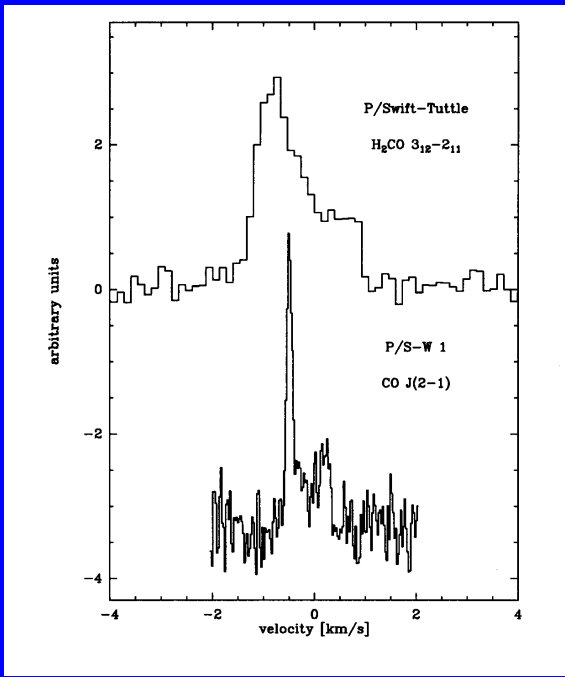

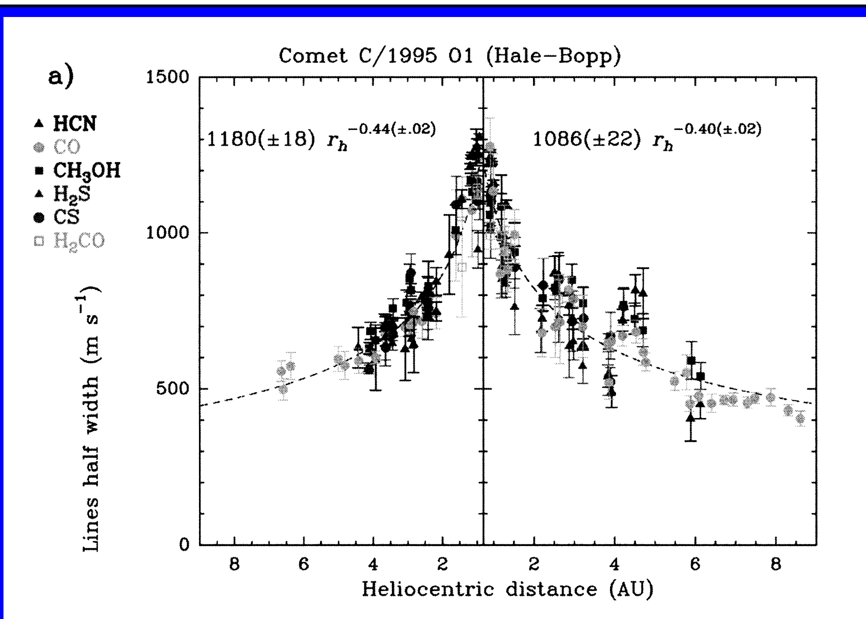

Figure 4. Upper plot: Velocity at half-maximum on the blue wing of the lines, which provides an estimate of the gas expansion velocity in comet Hale–Bopp. Fitted power laws are superimposed.

Gas outflow speed of comet Hale-Bopp, determined from radio observations.

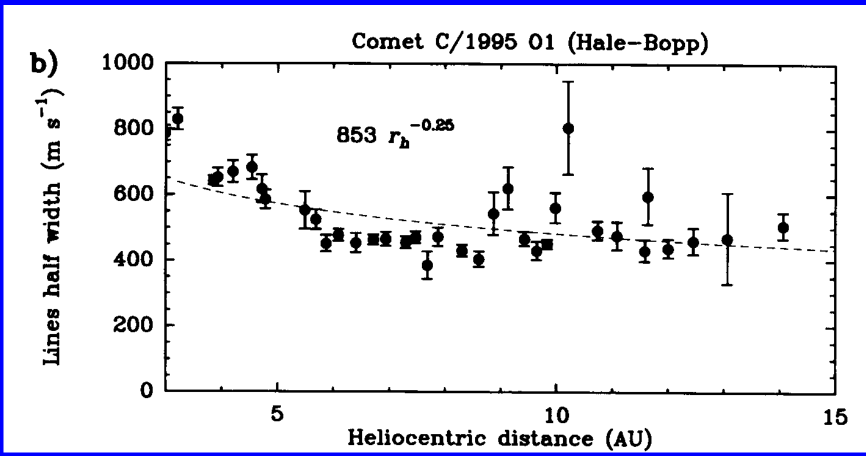

Velocity at half-maximum on the blue wing of the CO lines, beyond 3 AU postperihelion. A power law fit to these data is shown, but there are large deviations that suggest two distinct regimes, below and beyond 7 AU.
This and preceding slide from Biver et al.: The 1995-2002 long term monitoring of comet C/1995 O1 (Hale-Bopp) at radio wavelength. Earth, Moon and planets 90, 5-14, 2002.

Crovisier J., Solids and volatiles in comets: From cometary nuclei to cometary atmo-spheres, in Greenberg, Li eds., Formation and evolution of solids in space, Kluwer, 1999, 389-426.

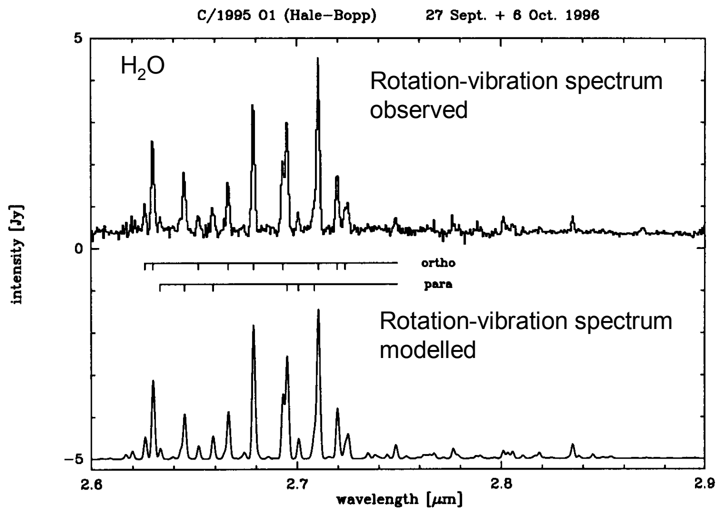

Figure 12. The spectrum of the 2.7 μm water band in comet C/1995 O1 (Hale-Bopp) observed by the short-wavelength spectrometer of *ISO* at 2.9 AU from the Sun. The resolution is $\lambda/\delta\lambda \sim 1500$ and the aperture is 14" × 20". The curve in the bottom shows a synthetic fluorescence spectrum of water computed for a rotational temperature of 28.5 K and an ortho-to-para ratio of 2.45. All the observed lines are due to water, except the line at 2.869 μm which is from OH (from [38]).

Rotation spectrum of water modelled.

This and the following slides are from Bockelée-Morvan and Crovisier, "Comets and asteroids with FIRST" in The promise of the Herschel Space Observatory, ESA-SP-460.

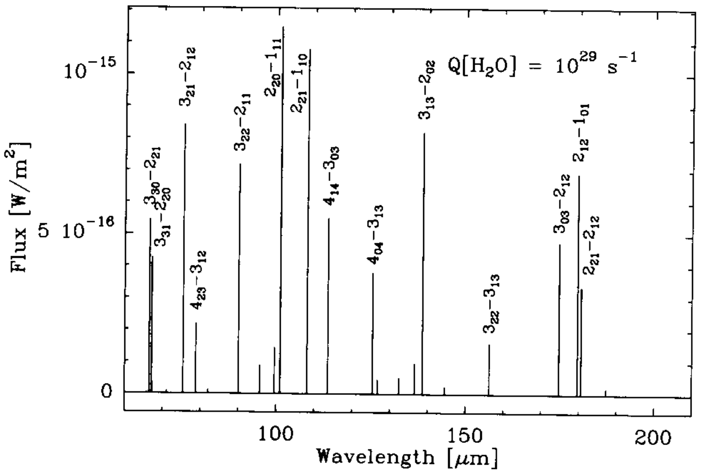

Figure 6. Synthetic spectrum of water for observations with PACS. Model and comet parameters are the same as for Fig. 4. The field-of-view diameter is taken to 9.4″.

Rotation spectrum of water observed in Comet Hale-Bopp (compare with prediction on previous slide).

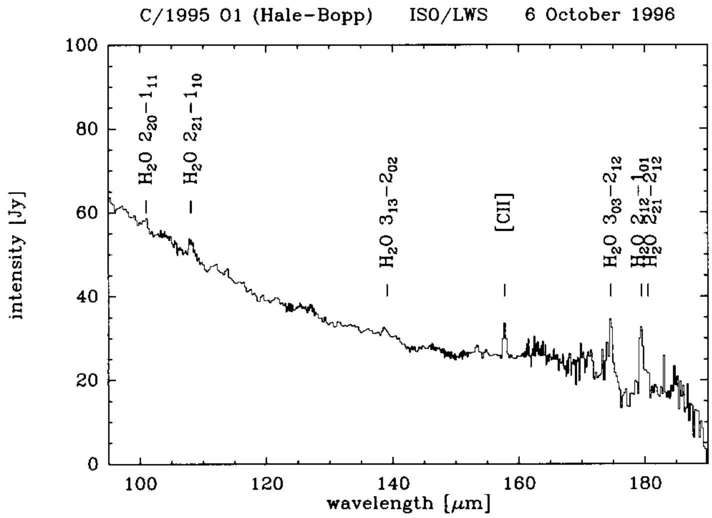

Figure 2. The rotational lines of water observed by the ISO long-wavelength spectrometer in comet Hale-Bopp at 2.9 AU from the Sun (Crovisier et al. 1999).

Low quantum number rotational lines of water (Model for comet with a water production Q = 10^{29} s^{-1}).

On next slide:
Model for Q = 10^{27} s^{-1}.

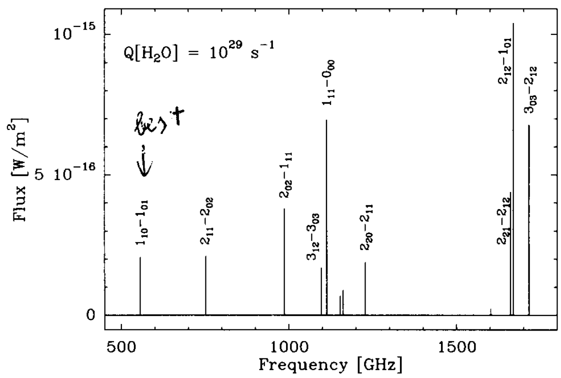

Figure 4. Synthetic spectrum of water for observations with HIFI and SPIRE. Intensities are computed for a comet at r_h = Δ = 1 AU with Q[H_2O] = 10^{29} molecules s^{-1} and FIRST diffraction limited beams. The excitation model of Bockelée-Morvan (1987) is used. Collisions with electrons are included (Biver et al. 1999a). The line transfer code for optically thick lines developped by Biver et al. (1999a) is used to compute the line intensities. The gas temperature and expansion velocity are taken equal to 60 K and 0.8 km s^{-1}, respectively.

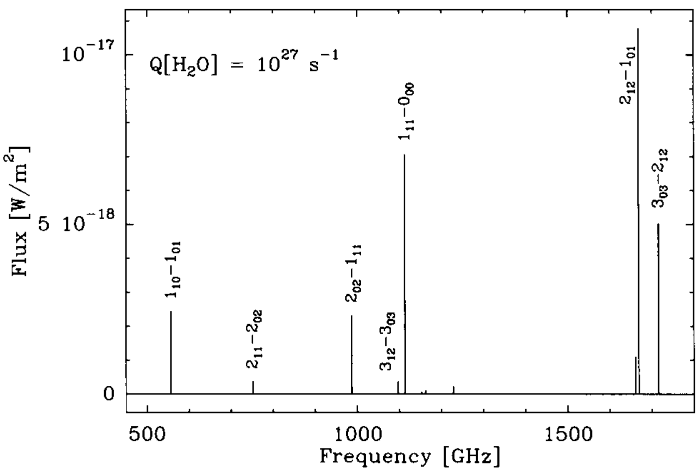

Figure 5. Synthetic spectrum of water for observations with HIFI and SPIRE. Model and comet parameters are the same as for Fig. 4, but with Q[H_2O] = 10^{27} molecules s^{-1}.

Self absorption predicted in blue wing of strong water line, because water outflow accelerates toward observer.

Next slide: same water line observed with the Odin satellite. The superimposed HCN line is optically thick. Predicted selfabsorption is confirmed by observation.

Lecacheux et al., A&A submitted.

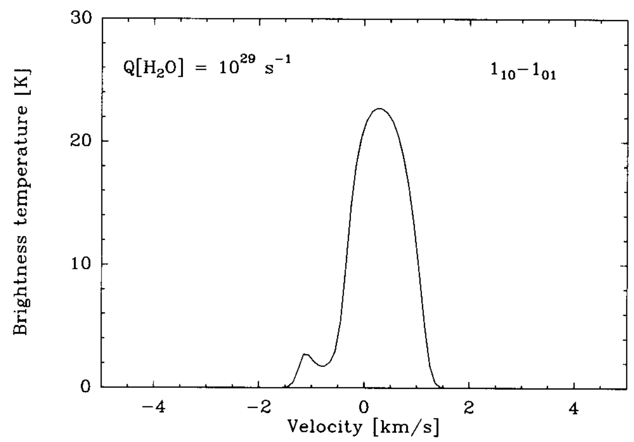

Figure 8. High resolution HIFI synthetic spectrum of the water 1_{10}–1_{01} line at 557 GHz. The model and comet parameters are the same as for Fig. 4. The line is asymmetric and has its centroid redshifted due to self-absorption in the front part of the coma. This illustrates the need of a high spectral resolution for understanding such line shapes.

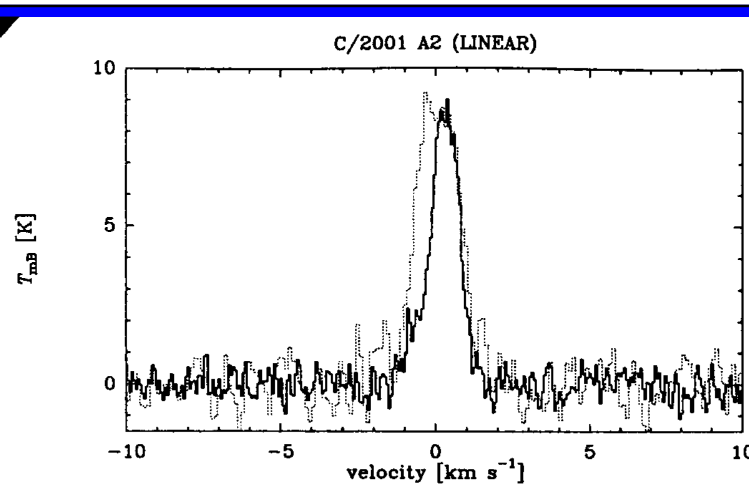

Fig. 1. The 1_{10}–1_{01} H_2O line at 557 GHz observed by Odin in comet C/2001 A2 (LINEAR) on 2.2 July 2001 (full line). For comparison, the *J*(3–2) line of HCN observed at the *CSO* is also shown (scale expanded by ×10, dotted line). The difference between the profiles is due to self-absorption in the water line.

OH Λ-type doubling at 18 cm.

de Pater and Lissauer, Planetary Sciences, Cambridge 2001.

Dependence of OH maser transition in the 18 cm wavelength band on cometary heliocentric velocity.

Maser is pumped by solar light at 309 nm (fundamental electronic band of OH.

OH is the most important dissociation product of water, from which the water production can be easily derived.

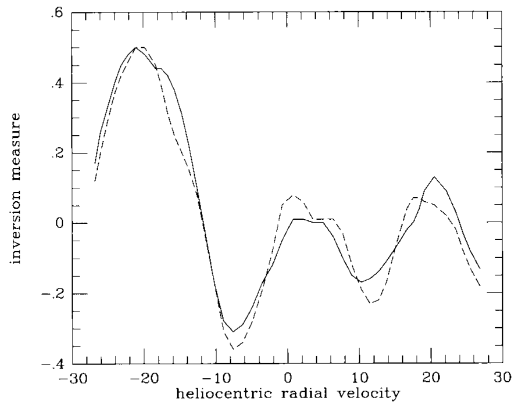

FIGURE 10.10 A graph of the inversion measure, $(n_u - n_l)/(n_u + n_l)$, for the OH transition at 1667 MHz, as a function of a comet's heliocentric velocity. When the inversion measure is positive, OH is seen in emission (maser); when the inversion measure is negative, OH is observed in absorption. The result for two pumping models are shown: ——, Despois *et al.* (1981) and – – – Schleicher (1983). (Adapted from de Pater *et al.* 1989)

Similar to previous slide, but this time the observation time of comet Kohoutek is plotted.

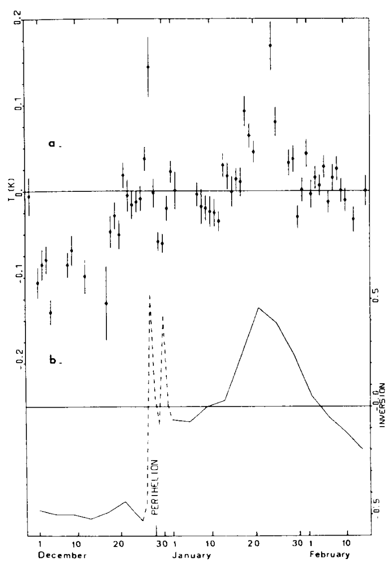

FIGURE 10.11 A comparison between radio OH data of C/Kohoutek in 1973–1974 (a) with the inversion measure predicted by the ultraviolet pumping model as a function of time (b). (Biraud *et al.* 1974)

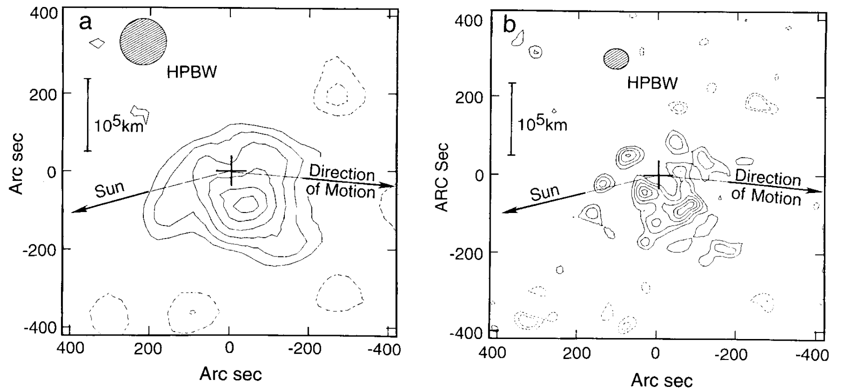

FIGURE 10.12 Radio image of the OH emission of P/Halley, taken at the peak flux density of the line (0.0 km s^{-1} in the reference frame of the comet). The cross in the center indicates the position of the nucleus. The shaded ellipse represents the resolution of the beam. Contour levels for the low-resolution image (a) are 4.9, 7.8, 10.8, 13.7, 16.7 and 18.6 mJy/beam; for the high resolution image (b) they are: 4.4, 6.0, 7.7, 9.3, and 10.4 mJy/beam. Dashed contours signify negative values (which are unphysical). (de Pater *et al.* 1986)

de Pater and Lissauer, Planetary Sciences, Cambridge 2001.
The OH maser line is forbidden and therefore long-living. Thus it is easily deexitated (quenched) by collisions. The reduced intensity at the nucleus in these images may be caused by this.

Crovisier J., in Greenberg, Li eds., Formation and evolution of solids in space, Kluwer, 1999, 389-426.

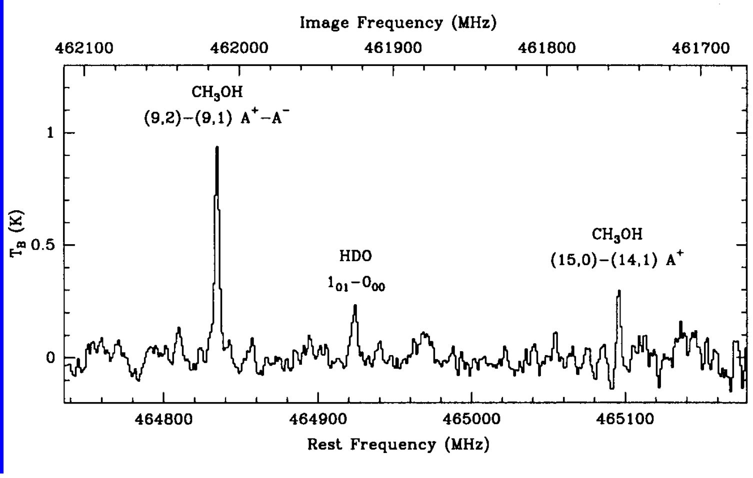

Figure 9. The $1_{10}-0_{00}$ HDO line at 465 GHz observed in comet C/1996 B2 (Hyakutake) at the Caltech Submillimeter Observatory. Two lines of methanol were observed in the same spectrum (from [13]).

The HDO transition observed in this spectrum corresponds to a very strongly forbidden ortho-para-transition in H2O which is allowed in HDO.

TABLE 10. Isotopic ratios in comets.

Isotopes		comet	method	cosmic	comet value	ref.
D/H	H_3O^+	1P/Halley	mass	1.5×10^{-5}	$3.08 \pm 0.53 \times 10^{-4}$	[8]
					$3.02 \pm 0.22 \times 10^{-4}$	[48]
	OH	1P/Halley	UV		$< 5 \times 10^{-4}$	[94]
	HDO	C/1990 K1	radio		$< 7 \times 10^{-3}$	[35]
		C/1996 B2	radio		$2.9 \pm 1.0 \times 10^{-4}$	[12]
		C/1995 O1	radio		$3.3 \pm 0.8 \times 10^{-4}$	[113]
$^{18}O/^{16}O$	H_3O^+	1P/Halley	mass	2.0×10^{-3}	$1.93 \pm 0.12 \times 10^{-3}$	[8]
					$2.13 \pm 0.18 \times 10^{-3}$	[48]
$^{13}C/^{12}C$	CN	1P/Halley	visible	1.1×10^{-2}	$1.05 \pm 0.13 \times 10^{-2}$	[71]
	HCN	C/1996 B2	radio		$2.9 \pm 1.0 \times 10^{-2}$	[77]
		C/1995 O1	radio		$1.11 \pm 0.18 \times 10^{-2}$	[78]
		C/1995 O1	radio		$0.90 \pm 0.09 \times 10^{-2}$	[80]
$^{15}N/^{14}N$	CN	1P/Halley	visible	3.6×10^{-3}	$< 3.6 \times 10^{-3}$	[71]
	HCN	C/1995 O1	radio		$3.1 \pm 0.4 \times 10^{-3}$	[80]
$^{34}S/^{32}S$		1P/Halley	mass	4.2×10^{-2}	$4.5 \pm 1.0 \times 10^{-2}$	[74]
	CS	C/1995 O1	radio		$3.7 \pm 0.4 \times 10^{-2}$	[80]

Crovisier J., in Greenberg, Li eds., Formation and evolution of solids in space, Kluwer, 1999, 389-426.

Solar system formation

- •Early stages (Ewine van Dieshoek, Leiden) a-d
- •A lot of steps between d and e:
- •Protoplanetary disk is hot near the Sun and cold far from the Sun, condensation of gas depending on temperature
- • Formation and growth of planetesimals (strongly dependent on relative velocity)
- • Formation of terrestrial and giant planets
- • Early Jupiter prevents planetesimal growth in its neighborhood → origin of asteroids
- • Comets originate in the Kuiper belt at about 40 AU from the Sun
- •Long-period comets are scattered into Oort cloud, disturbed and isotropized by the influence of passing stars and the galactic bulge.
- •Short-period comets go directly from Kuiper belt to the inner solar system
- •Meteorites come from the surfaces of asteroids and from Mars to the Earth. Their measurement in the laboratory has contributed greatly to our knowledge about solar system formation.

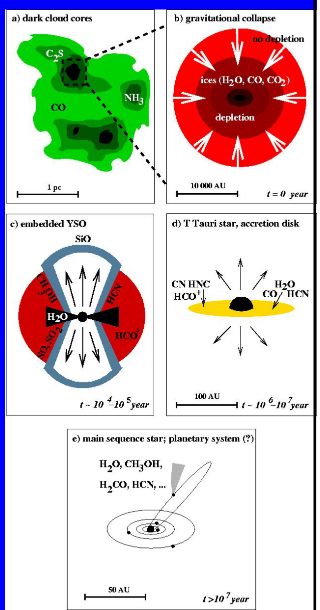

D/H ratios in the solar system, from Hersant F. et al., Astrophys. J. 554, 391-407, 2001.

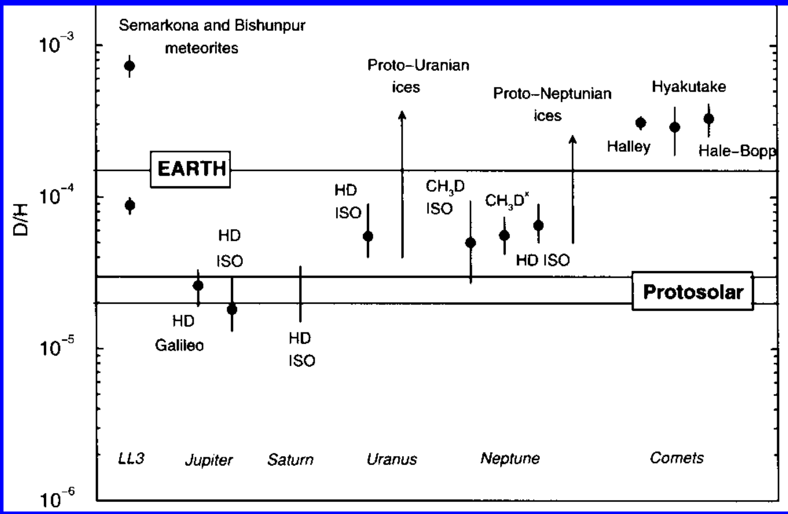

According to these authors, interstellar icy grains with high D/H ratio remained unprocessed during the formation of the protosolar nebula. They are found unprocessed in LL3 meteorites like Semarkona and Bishunpur. Otherwise they were mixed into a protosolar cloud with D/H = 2.5 10^{-5} with mixing ratio depending on heliocentric distance.

How to calculate production rates?

1. Parent – daughter concept with lifetime of parent and daughter, ejection velocity of parent, extra speed of daughter (based on molecular and solar data)

2. Getting the number of molecules in the beam (field of view) from the observation of a singular line or band:
• fluorescence: with a calculation of the complete excitation model involving all important transitions (g-factor)
• collisional equilibrium: assuming Boltzmann distribution

3. Estimation of the fraction of molecules in the beam (field of view) using models of various kinds: Haser (radial outflow), Festou, Combi and Delsemme (“vectorial” model)

4. Production rate = total number of molecules/life time

Haser model

(Haser 1957, Bull. Acad. R. Belgique Classe des Sciences 43, 740-750)

Equations for parent molecule

$$\mathrm{D}(r) = \mathrm{D}(r_0) \cdot \left(\frac{r_0}{r}\right)^{-2} \cdot \exp \cdot \left[-\frac{t - t_0}{\tau_0}\right]$$

D: density, *r*: distance from nucleus, *t*: time, τ_0: life time of parent, v_0: ejection speed of parent

$v_0\tau_0$ scale length of parent

$$t = \frac{r}{v_0} \qquad \mathrm{D}(r) = \mathrm{D}(r_0) \cdot \left[\frac{r_0}{r}\right]^2 \cdot \exp . \left[-\frac{r - r_0}{v_0\tau_0}\right] \qquad (1)$$

Integration along line of sight in order to derive observable column densities

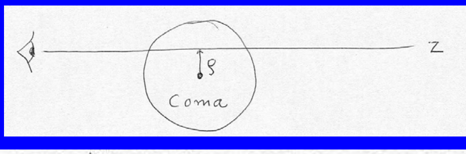

$$\mathrm{J}(\rho) = \mathrm{D}(r_0) \cdot r_0^2 \cdot \exp. \left[\frac{r_0}{v_0\tau_0}\right] \int_{-\infty}^{+\infty} \frac{1}{r^2} \cdot \exp. \left[-\frac{r}{v_0\tau_0}\right] dz \qquad (2)$$

Integral leads to Bessel functions

Haser model

(Haser 1957, Bull. Acad. R. Belgique Classe des Sciences 43, 740-750)

Equations for daughter molecule

$$\beta_0 = \frac{1}{v_0\tau_0}$$ Inverse parent scale length

$$\beta_1 = \frac{1}{v_1\tau_1}$$ Inverse daughter scale length

D1: density of daughter species

$$\mathrm{D}_1(r) = \mathrm{D}(r_0) \frac{v_0}{v_1} \left[\frac{r_0}{r}\right]^2 \beta_0 \frac{\exp.[-\beta_0(r - r_0)] - \exp.[-\beta_1(r - r_0)]}{\beta_1 - \beta_0} \qquad (9)$$